Available online at www.sciencedirect.com
ScienceDirect
Journal of Physics and Chemistry of Solids 68 (2007) 586–593
JOURNAL OF PHYSICS AND CHEMISTRY OF SOLIDS
www.elsevier.com/locate/jpcs

Growth, EPR and optical absorption spectra of L-threonine single crystals doped with Cu^{2+} ions

R.C. Santana[a,*], R.O. Cunha[a], M.G. Santos[a], K.D. Ferreira[a], J.F. Carvalho[a], R. Calvo[b]

[a]*Instituto de Física, Universidade Federal de Goiás, Campus Samambaia, CP 131, 74001-970 Goiânia (GO), Brazil*
[b]*Departamento de Física, Facultad de Bioquímica y Ciencias Biológicas, Universidad Nacional del Litoral, INTEC (CONICET-UNL), Güemes 3450, 3000 Santa Fe, Argentina*

Received 1 November 2006; received in revised form 28 December 2006; accepted 23 January 2007

Abstract

We investigated the crystal growth, electron paramagnetic resonance (EPR) and optical absorption spectra of L-threonine doped with Cu^{2+}. The quality, size and habit of the single crystals grown from aqueous solution by the slow solvent evaporation and by the cooling methods vary when the impurities are introduced during the growth process. The variations with the magnetic field orientation of the EPR spectra of single-crystal samples at room temperature and 9.77 GHz in three crystal planes (*ab*, *bc* and *ac*) show the presence of copper impurities in four symmetry-related sites of the unit cell. These spectra display well resolved hyperfine couplings of the $S=\frac{1}{2}$ of Cu^{2+} with the $I_{Cu}=\frac{3}{2}$ of the copper nuclei. Additional hyperfine splittings, well-resolved only for specific orientations of the magnetic field, indicate that the copper impurity ions in the interstitial sites have two N ligands with similar hyperfine couplings. The principal values of the $\boldsymbol{g}$ and $\boldsymbol{A}_{Cu}$ tensors calculated from the EPR data are $g_1=2.051(1)$, $g_2=2.062(2)$, $g_3=2.260(2)$, $A_{Cu,1}=16.9(5)\times10^{-4}\,cm^{-1}$, $A_{Cu,2}=21.8(6)\times10^{-4}\,cm^{-1}$, $A_{Cu,3}=180.0(5)\times10^{-4}\,cm^{-1}$. The principal directions corresponding to g_3 and to $A_{Cu,3}$ are coincident within the experimental errors, reflecting the orientation of the bonding planes of the copper ions in the crystal. The values of the crystal field energies are evaluated from the optical absorption spectrum, and the crystal field and bonding parameters of the Cu impurities in the crystal are calculated and analyzed. The EPR and optical absorption results are discussed in terms of the crystal structure of L-threonine and the electronic structure of the Cu^{2+} ions, and compared with data reported for other systems. The effects of the impurities in the growth and habit of the crystals are also discussed.
© 2007 Elsevier Ltd. All rights reserved.

PACS: 76.30.Fc; 71.70.Ch

Keywords: A. Organic compound; B. Crystal growth; D. Electron paramagnetic resonance (EPR); D. Crystal fields

1. Introduction

Single crystals of amino acids such as L-arginine, L-alanine and L-threonine, display interesting physical properties as second harmonic generator (SHG), high nonlinearity, high damage threshold, and low refractive indices [1–3]. These properties make them convenient materials for applications in the field of telecommunications, optical information storing devices and as potential materials for second harmonic generation in high power laser systems.

Metal ions introduced as minor impurities during the crystal growth may have important consequences on the growth kinetics, morphology and quality of the crystals, improving in many cases their physical properties for specific applications. Recently, Dhanuskodi et al. [4] studied the non-linear optical crystal L-arginine sulphophosphate doped with Cu^{2+} and VO^{2+} ions. They reported that, as a consequence of the increased covalence and electron delocalization due to the doping, the SHG efficiency of doped crystals is higher than that of the pure ones. Thus, it is interesting to study the structural details and the microscopic processes occurring in the crystal when they are doped with metal ions, particularly in cases where

*Corresponding author. Tel.: +55 62 3521 1014; fax: +55 62 3521 1014.
E-mail address: santana@if.ufg.br (R.C. Santana).

0022-3697/$ - see front matter © 2007 Elsevier Ltd. All rights reserved.
doi:10.1016/j.jpcs.2007.01.043

these metal ions can be used as probes for spectroscopic techniques.

The peculiar physical and chemical properties of amino acids in the solid state are associated to their dipolar nature [5]. This is the case of crystalline L-threonine where the amino acid molecule is deprotonated at the carboxyl group and protonated at the amino group [6]. The crystal structure of L-threonine, $C_4H_9NO_3$, was determined by Shoemaker et al. [7], and later refined by Ramanadham et al. [6] and Janczak et al. [8]. It is orthorhombic with space group $P2_12_12_1$, lattice parameters $a = 13.628(2)$ Å, $b = 7.618(1)$ Å, and $c = 5.110(1)$ Å and have four formula units per unit cell ($Z = 4$). Investigations concerning the growth, structure, thermal and optical properties, vibrational spectroscopy, and more specifically SHG of pure L-threonine crystals have been reported [3, 9–13]. To our knowledge, however, no studies exist of the changes on the crystal growth and the properties of L-threonine produced by doping with copper ions.

In this investigation we report the growth of copper doped L-threonine single crystals having good optical quality and study them using EPR and optical absorption techniques, which provide information about the electronic structure, oxidation state, site symmetry and the bonding nature of the impurity ions. Cu^{2+} ions are of particular interest because they can be easily detected by EPR and their $3d^9$ electronic configuration allows modeling the local environment of the impurities, and performing detailed bonding studies.

2. Experimental section

Crystal growth solutions were prepared by dissolving 0.10 mol (12.000 g) of the amino acid L-threonine (Ajinomoto Co.) and 4.84 mmol (1.209 g) of copper sulphate pentahydrate, $CuSO_4.5H_2O$ (Vetec), in 100 ml of distilled water. The solutions were heated to 60 °C while agitated with a magnetic stirring device, and filtered after complete dissolution of the starting materials, when their pH was about 3.0. Single crystals were obtained by both, evaporation and cooling methods. A sealed chamber inside a thermal bath whose temperature was controlled by a Eurotherm 2416 microprocessor-based digital temperature controller allowing cooling rates of about 0.2 °C/day, was used in crystal growth by slow cooling. In this case the temperature ranged from 35 to about 29 °C.

Single-crystal EPR spectra were obtained with a Bruker ESP-300 spectrometer operating at 9.77 GHz, equipped with a standard rectangular cavity. The microwave frequency was measured with a Hewlett-Packard 5350B microwave counter. The magnetic field was calibrated using DPPH ($g = 2.0036$) as field marker positioned close to the sample. The EPR spectrum of a powdered sample made by finely grinding single crystals was measured with a VARIAN E-109 spectrometer operating at 9.51 GHz. Both spectrometers use a magnetic field modulation of 100 kHz. All EPR data were obtained at room temperature. The orientation of the single crystal samples for the EPR measurements was attained by gluing them to appropriate holders (described later) that allowed measuring the EPR spectra of the samples with the magnetic field at 5° intervals in a range of 180°, in the orthogonal crystal planes *ab*, *ca* and *cb*. The position of the orthorhombic axes ***a***, ***b*** and ***c*** in these planes was determined within ~1° from the angular variation of the spectra which follows the symmetry properties of the crystal.

Optical absorption spectra were recorded at room temperature on a Cary 50 Spectrophotometer. X-ray powder diffraction studies were carried out with a Shimadzu XRD-6000 diffractometer using CuK_α radiation. The crystal morphology was investigated using goniometric measurements and X-ray Laue pictures.

3. Results

3.1. Crystal growth

Light blue single crystals of copper doped L-threonine (hereafter called L-thr:Cu^{2+}), see Fig. 1a, were obtained by both, evaporation and cooling methods. Small crystals with dimensions of about $3 \times 1 \times 1\,mm^3$ obtained by evaporation were used for the EPR measurements and as seeds for the crystal growth by the slow cooling method that allowed obtaining crystals with dimensions up to $16 \times 2 \times 2\,mm^3$. Pure and doped crystals showed identical X-ray powder diffraction profiles reflecting the structural information reported by Janczak et al. [8] for pure L-threonine. The copper concentration in the crystals measured by atomic absorption spectroscopy is about 200 ppm.

Our investigation shows that copper impurities modify the crystal growth habit of L-threonine. The growth habit of pure crystals is characterized by predominant {1 1 0}, {1 2 0} and {0 1 1} faces and the crystals are elongated in the ***c***-direction [14]. On the other side, copper doped crystals display predominant {2 1 0} faces on the prismatic zone, and only few crystals showed vestigial {1 1 0}, {1 2 0} and {1 0 0} faces. The elongation in the ***c***-direction and the {0 1 1} faces remains unchanged in doped crystals. A photography of an as-grown doped crystal and a schematic view of their crystal habit are displayed in Figs. 1a and 1b, respectively. The single crystal samples for the EPR measurements were oriented considering this habit, by gluing a (2 1 0) face to a sample holder made of rexolite, shown in Fig. 1c, where the angle α was calculated from the structural information. This holder defines a set of orthogonal axes $\boldsymbol{x} \equiv \boldsymbol{a}$, $\boldsymbol{y} \equiv \boldsymbol{b}$ and $\boldsymbol{z} \equiv \boldsymbol{c}$, and was mounted on top of a goniometer placed inside of the microwave cavity to allow for the magnetic field rotations described before.

3.2. EPR data and analysis

The observed powder EPR spectrum, displayed in Fig. 2a, is typical of samples doped with small concentrations of copper ions [15] in a local environment that is not

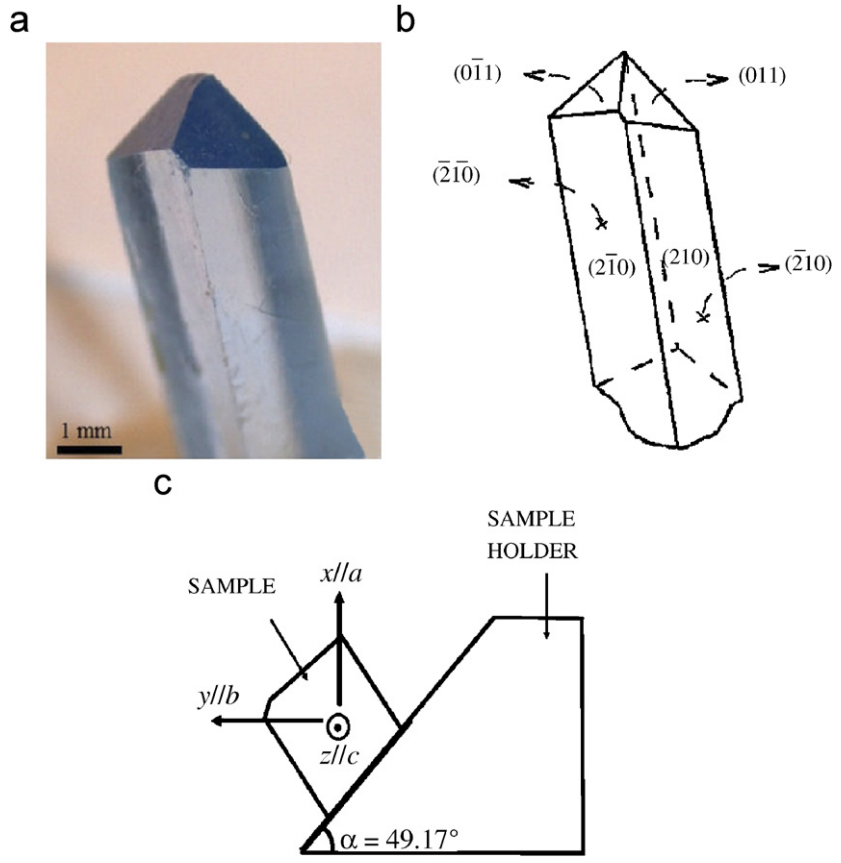

Fig. 1. (a) Photography of a L-thr:Cu^{2+} single crystal grown from aqueous solution by the slow evaporation method. (b) Growth morphology of L-thr:Cu^{2+} crystals shown in (a). (c) Sample holder used to mount the single-crystals for the EPR experiments.

far from square planar or octahedral. The low field region shows resolved hyperfine structure with the nuclear spin of copper. The high field region shows splittings which may be attributed to superhyperfine couplings with the nuclear spins of ligands. The EPR spectrum of the powder sample was simulated using the SIM-PIP program [16], considering the presence of the two natural copper isotopes ($I_{Cu} = 3/2$) with their natural abundances and two ^{14}N nucleus ($I = 1$), proposing an isotropic Gaussian derivative line shape.

Figs. 3a and b display EPR spectra of an L-thr:Cu^{2+} single crystal with the magnetic field applied along the ***a***-axis (Fig. 3a), and at 4° from the ***a***-axis in the *ab* plane (Fig. 3b). Along the crystal axes (Fig. 3a) the spectrum displays a single set of four similar hyperfine components arising from the coupling of the $S = \frac{1}{2}$ electronic spin of copper, with its nuclear spin $I_{Cu} = \frac{3}{2}$. Two four-line sets are observed for other orientations of the magnetic field in the crystal planes (Fig. 3b). They are attributed to copper impurities in four symmetry-related sites which, according to the properties of the crystallographic space group, should give EPR spectra coincident by pairs in the crystallographic planes [17]. Since the two natural copper isotopes have different magnetic moments, hyperfine and superhyperfine patterns are not clearly resolved for most orientations of the magnetic field.

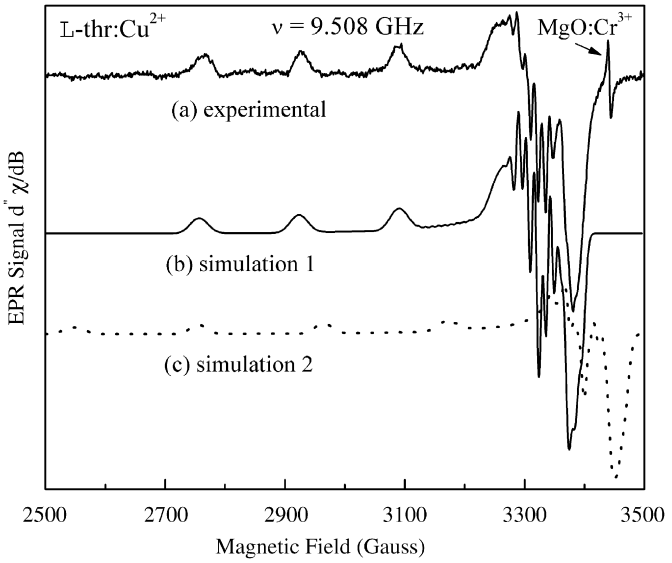

Fig. 2. (a) EPR spectrum observed for a powder sample of L-thr:Cu^{2+}. (b) Spectrum simulated with the set I of spin Hamiltonian parameters (Table 1), obtained from the single-crystal data. The sharp lines in the high field region are due to superhyperfine interaction with the nuclear spins of nitrogen ligands. The values of A_N used in the simulations are given in the text. (c) Spectrum simulated with the set II of parameters obtained from the single-crystal data, arising from a wrong assignment of the resonances in different planes (see text). For convenience, a MgO:Cr^{3+} sample was used here for magnetic field calibration.

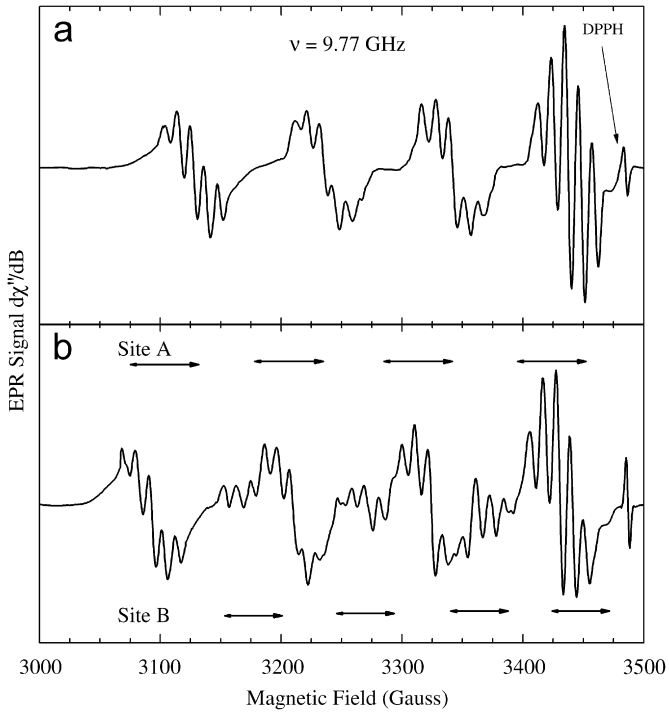

Fig. 3. EPR spectra of Cu^{2+} impurities in a L-threonine single crystal: (a) Spectrum showing four group of resonances observed for $\boldsymbol{B}//\boldsymbol{a}$. (b) Spectrum showing eight groups of resonance lines observed at 4° from the $\boldsymbol{a}$ axis in the *ab* plane. These spectra have additional superhyperfine splittings arising from two nitrogen ligands.

For certain magnetic field directions the observed resonances are further split in five components which are attributed to the superhyperfine interaction of the electronic spin of copper with the nuclear spins of two ^{14}N ligands ($I_N = 1$) with similar hyperfine couplings, in *trans* positions (see for example Fig. 3a). The spectra become more complicate when the magnetic field is applied in a general orientation, indicating that the hyperfine coupling constants of the two ^{14}N ligands are not equal. This is expected as a consequence of the absence of sites having inversion symmetry in the $P_{2_12_12_1}$ space group of threonine.

The spin Hamiltonian describing the energy levels of the Cu^{2+} ions is

$$H = \sum_{\alpha=\mathrm{I\text{-}IV}} \left(\mu_B \boldsymbol{S}_\alpha \cdot \boldsymbol{g}_\alpha \cdot \boldsymbol{B} + \boldsymbol{I}_\alpha \cdot \boldsymbol{A}_{\mathrm{Cu},\alpha} \cdot \boldsymbol{S}_\alpha + \sum_{i=1,2} \boldsymbol{I}_{N_{\alpha,i}} \cdot \boldsymbol{A}_{N_{\alpha,i}} \cdot \boldsymbol{S}_\alpha \right), \quad (1)$$

where μ_B is the Bohr magneton, $\boldsymbol{g}_\alpha$, $\boldsymbol{A}_{\mathrm{Cu},\alpha}$, and $\boldsymbol{A}_{N_{\alpha i}}$ are the g, copper hyperfine, and nitrogen hyperfine tensors (i labels the N atoms), respectively, for copper ions in site α (α = I–IV) of the structure of L-threonine. The first term on the right hand side of Eq. (1) is the Zeeman interaction of the effective spin $S =$ of copper ions with the applied magnetic field $\boldsymbol{B}$. The second and third terms represent the hyperfine interaction of the electron spin with the nuclear spins of Cu_α ($\boldsymbol{I}_{Cu_\alpha}$) and the N ($\boldsymbol{I}_{N_{\alpha i}}$) ligands, respectively. As required by the space symmetry of L-threonine, the tensors $\boldsymbol{g}_\alpha$ and $\boldsymbol{A}_{\mathrm{Cu},\alpha}$ for different α are related by C_2 rotations around the crystal axes.

To analyze the single-crystal EPR data and calculate the tensors $\boldsymbol{g}$ and $\boldsymbol{A}_{Cu}$ defined in Eq. (1), we followed the method described in Ref. [17]. First, we calculated from the single-crystal spectra the first order values of $g(\theta,\varphi)$ and $A_{Cu}(\theta,\varphi)$ as a function of magnetic field orientation $\boldsymbol{h} = \boldsymbol{B}/|\boldsymbol{B}| = (\sin\theta\ \cos\varphi,\ \sin\theta\ \sin\varphi,\ \cos\theta)$ from the average position $[g(\theta,\varphi)]$ and the average splitting $[A_{Cu}(\theta,\varphi)]$, respectively, of each Cu-hyperfine resonance. In cases where a ligand superhyperfine splitting of the lines exists, the positions of the Cu-hyperfine resonances were taken at the average magnetic field over the nitrogen hyperfine group. These values of $g(\theta,\varphi)$ and $A_{Cu}(\theta,\varphi)$ are valid up to first order in a perturbative expansion of the spin Hamiltonian energies in powers of $A_{Cu}(\theta,\phi)/[g(\theta,\varphi)\mu_B B]$ (see Ref. [18]). They allowed to calculate the angular variations of $g^2(\theta,\varphi)$ and $g^2\ A^2_{Cu}\ (\theta,\varphi)$ in the crystalline planes *ab*, ca and *cb*, shown by symbols in Figs. 4a and b. Thus, first order values of the components of the tensors $\boldsymbol{g}.\boldsymbol{g}$ and $\boldsymbol{g}.\boldsymbol{A}_{Cu}.\boldsymbol{A}_{Cu}.\boldsymbol{g}$ were obtained by least squares fits of these values of $g^2(\theta,\varphi)$ and $g^2\ A^2_{Cu}\ (\theta,\varphi)$. These tensors were used to calculate the second order perturbation corrections using the expansions up to second order given by Weil [18].

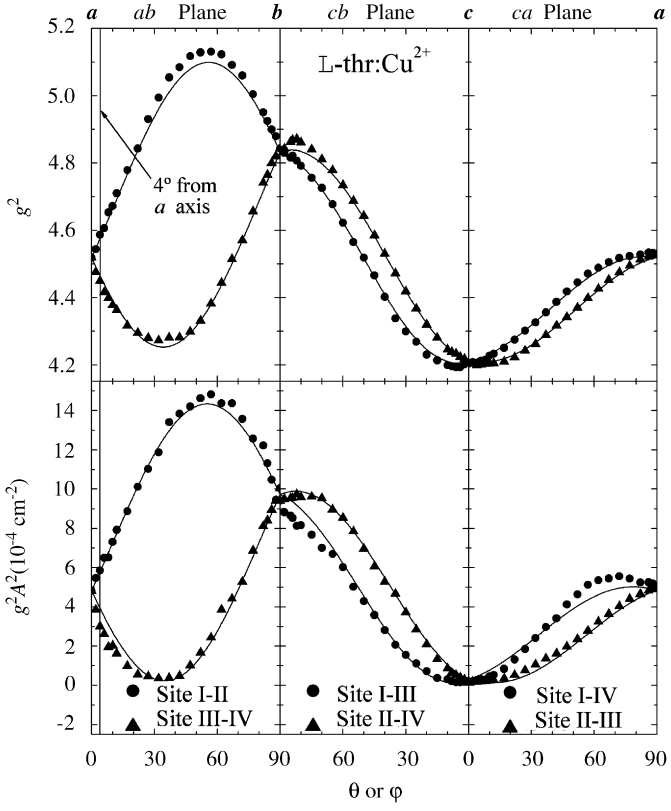

Fig. 4. Angular variation of (a) $g^2(\theta,\varphi)$ and (b) $g^2A^2(\theta,\varphi)$ calculated in the planes *ab*, ca, *cb* (symbols). The solid lines were obtained with the components of the $\boldsymbol{g}.\boldsymbol{g}$ and $\boldsymbol{g}.\boldsymbol{A}_{Cu}.\boldsymbol{A}_{Cu}.\boldsymbol{g}$ tensors given in Table 1 (see text). The vertical line at 4° in the *ab* plane indicates the orientation where the spectrum shown in Fig. 3b was obtained.

The analysis was completed following the iterative self-consistent procedure described in [17] that allowed us to obtain the components of the tensors $\boldsymbol{g}.\boldsymbol{g}$ and $\boldsymbol{g}.\boldsymbol{A}_{Cu}.\boldsymbol{A}_{Cu}.\boldsymbol{g}$ valid up to second order correction terms. These second order corrections have magnitudes comparable to the experimental uncertainties.

It is important to consider that there are eight different possibilities to assign the two sets of resonances observed in each studied plane. They give rise to eight possible sets of values for the spin Hamiltonian parameters that differ only in the signs of the nondiagonal parameters. As explained by Massa et al. [19], these eight tensors may be divided into two sets of four symmetry related tensors (called sets I and II), having each set the same eigenvalues. To choose the physically correct set of four $\boldsymbol{g}.\boldsymbol{g}$ and $\boldsymbol{g}.\boldsymbol{A}_{Cu}.\boldsymbol{A}_{Cu}.\boldsymbol{g}$ tensors corresponding to the four symmetry related sites of the Cu impurities in the structure, one compares the observed powder spectrum with those simulated using each set of spin Hamiltonian parameters. Both sets, I and II, display approximate axial symmetry for the $\boldsymbol{g}$-tensor, but only set I reproduces the observed powder spectrum (see Figs. 2a and b) and was considered the correct solution corresponding to four symmetry related lattice sites for the copper impurities (see discussion of a similar situation in Ref. [19]). The set II does not reproduce the powder spectrum and arises from a wrong assignment of the resonances in the three studied sample planes (see Fig. 2c). To avoid this double solution to the problem, measurements in a fourth plane should be needed. This is avoided here by the simulation of the powder spectrum. Table 1 contains the values of the components of the $\boldsymbol{g}$ and $\boldsymbol{A}_{Cu}$ tensors obtained from the single-crystal data, that reproduce the powder spectrum (set I). This table also includes their eigenvalues and eigenvectors referred to the orthogonal set of laboratory axes $\boldsymbol{xyz} \equiv \boldsymbol{abc}$. The solid lines in Figs. 4a and 4b were calculated with these values, which reflect the properties of the host lattice and the characteristics of the copper ions. The chosen assignment of the resonances, leading to the solution I is indicated in Figs. 4a and b.

The magnitudes of the superhyperfine coupling parameter $\boldsymbol{A}_{N_{zi}}$ ($i = 1, 2$), were assumed equal and estimated in two directions of the applied magnetic field from simulations of the experimental spectra, assuming Gaussian derivative line shapes for the two N ligands with equal coupling, as obtained for *trans* coordination if approximate inversion symmetry around the copper ions is assumed. Fig. 5 displays these simulations for the low field groups of lines of the spectra observed for $\boldsymbol{B}$ along the $\boldsymbol{a}$-axis (Fig. 5a) and for $\boldsymbol{B}$ at 4° from the $\boldsymbol{a}$-axis in the *ab* plane (Fig. 5b). The values of the nitrogen superhyperfine coupling constants A_{N_z} obtained from these simulations are A_{N1}-$A_{N2} = 10.1 \times 10^{-4}\,cm^{-1}$ for $\boldsymbol{B}$ along the $\boldsymbol{a}$-axis, and $A_{N1} = A_{N2} = 9.9 \times 10^{-4}\,cm^{-1}$ for $\boldsymbol{B}$ at 4° from $\boldsymbol{a}$-axis in the *ab* plane. However, due to the overlapping of the resonances we were not able to measure the full angular variation of the superhyperfine interaction, as required to evaluate all components of the nitrogen hyperfine tensors.

Table 1
Components of the $\boldsymbol{g}^2$ (a) and $\boldsymbol{g}^2\boldsymbol{A}^2$ tensors (b) obtained from a least squares analysis of the values in Figs. 4a,b, as explained in the text. (c) and (d) Eigenvalues and eigenvectors of the tensors $\boldsymbol{g}$ and $\boldsymbol{A}_{Cu}$

(a) $\boldsymbol{g}^2$ tensor	
$(g^2)_{xx} = 4.519(1)$	$(g^2)_{xy} = 0.396(2)$
$(g^2)_{yy} = 4.833(1)$	$(g^2)_{xz} = 0.035(2)$
$(g^2)_{zz} = 4.211(1)$	$(g^2)_{yz} = 0.061(2)$
(b) $\boldsymbol{g}^2\boldsymbol{A}^2$ tensor ($\times 10^{-4}\,cm^{-2}$)	
$(g^2A^2)_{xx} = 4.84(5)$	$(g^2A^2)_{xy} = 6.66(6)$
$(g^2A^2)_{yy} = 9.73(5)$	$(g^2A^2)_{xz} = 0.95(6)$
$(g^2A^2)_{zz} = 0.31(5)$	$(g^2A^2)_{yz} = 1.31(6)$
(c) *Eigenvalues*	*Eigenvectors*
$g_1 = 2.051(1)$	(0.053(9), −0.130(9), 0.990(4))
$g_2 = 2.062(2)$	(0.827(2), −0.549(5), −0.121(9))
$g_3 = 2.260(2)$	(0.560(1), 0.825(1), 0.078(2))
(d) *Eigenvalues* ($\times 10^{-4}\,cm^{-1}$)	*Eigenvectors*
$A_{Cu,1} = 16.9(5)$	(0.355(9), −0.119(9), −0.927(6))
$A_{Cu,2} = 21.8(6)$	(0.742(9), −0.568(2), 0.356(9))
$A_{Cu,3} = 180.0(6)$	(0.569(1), 0.815(1), 0.113(3))

$\boldsymbol{x} \equiv \boldsymbol{a}$, $\boldsymbol{y} \equiv \boldsymbol{b}$, $\boldsymbol{z} \equiv \boldsymbol{c}$. The uncertainties of the eigenvalues and eigenvectors were calculated from those obtained from the least-squares fit of the components of the $\boldsymbol{g}^2$ and $\boldsymbol{g}^2\boldsymbol{A}^2$ tensors shown in (a) and (b).

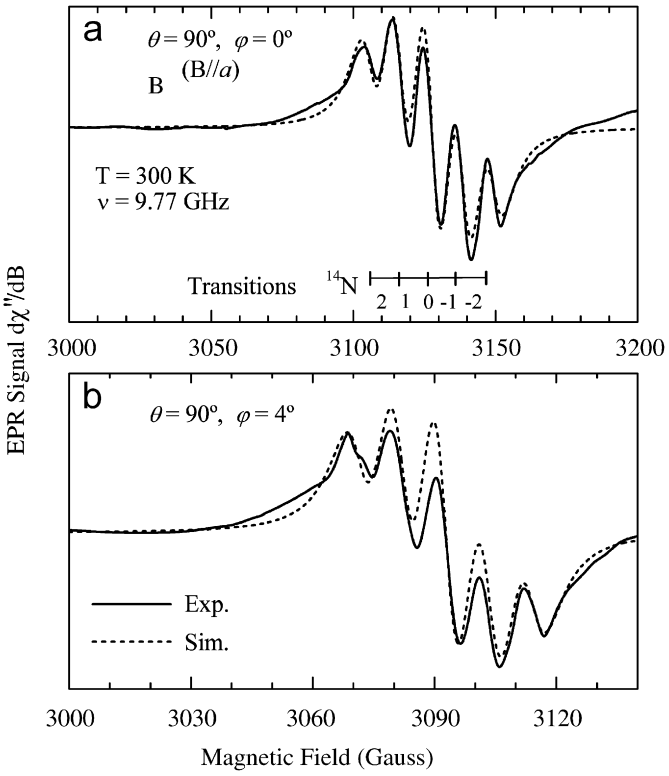

Fig. 5. ^{14}N ligand superhyperfine splittings observed for the low field groups of resonances of Figs. 3a and b. Solid lines are experimental results; dotted lines are simulations obtained as explained in the text. (a) $\boldsymbol{B}//\boldsymbol{a}$ axis, and (b) $\boldsymbol{B}$ at 4° from the $\boldsymbol{a}$-axis, in the *ab* plane.

3.3. Analysis of the optical spectrum

The optical absorption spectrum of a crystal of L-thr:Cu^{2+} recorded at room temperature, Fig. 6, shows one broad band centered at 730 nm. This band, characteristic of Cu^{2+} ions in rhombic symmetry [20], is the sum of three overlapping bands corresponding to the *d–d* copper electronic transitions E_{xy} ($^2B_{1g}\rightarrow{}^2B_{2g}$), $E_{xz,yz}$ ($^2B_{1g}\rightarrow{}^2E_g$) and E_{z^2} ($^2B_{1g}\rightarrow{}^2A_{1g}$). The position of each band, obtained from simulations with Gaussian functions (see Fig. 6), are $E_{xy}=14{,}165\pm32\,cm^{-1}$, $E_{xz,yz}=18{,}199\pm27\,cm^{-1}$, $E_{z^2}=11{,}722\pm30\,cm^{-1}$. From these values and using the equations given by Ballhausen [20], we calculated the octahedral (D_q) and tetragonal (D_s and D_t) crystal field parameters listed in Table 2. In that table, the values obtained are compared to those reported by Salagram et al. [21] for Cu^{2+} ions in $Sr(HCOO)_2\cdot2H_2O$, by Tovar–Tovar et al. [22] for [Cu(4,4'-dimethyl-2,2′-bipyridine)(acetylacetonate)NO_3], called Cas III ia NO_3, and by Dhanuskodi et al. [23] for Cu^{2+} doped L-arginine sulpho phosphate monohydrate (LASP), where the D_s parameter suggests that the crystal field at the Cu^{2+} site in all crystals under consideration is highly distorted.

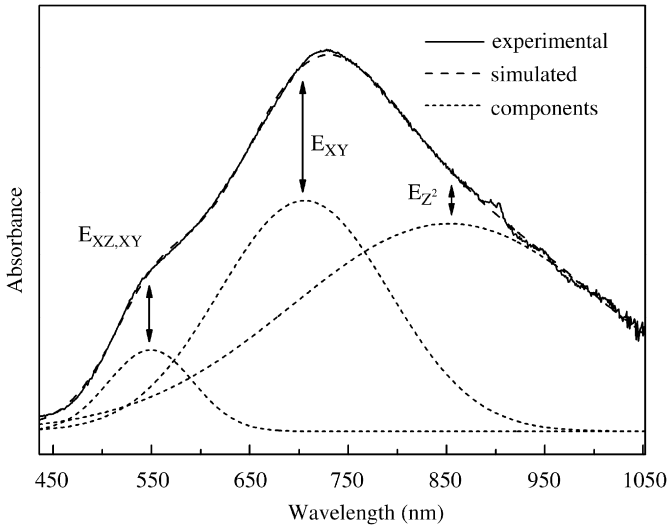

Fig. 6. Electronic absorption spectrum of a L-thr:Cu^{2+} single crystal at room temperature. This spectrum is decomposed as the sum of three Gaussian components corresponding to the electronic transitions (see text).

Table 2
Crystal field parameters (cm^{-1}) for Cu^{2+} impurities in L-threonine and in other hosts

Sample	D_q	D_t	D_s	Ref.
L-threonine	1417±4	554±3	2251±4	This work
$Sr(HCOO)_2.2H_2O$	1290	40	2638	[21]
Cas III ia NO_3	1645	897	2350	[22]
LASP	1075	217	2179	[23]

The uncertainties of the values for L-threonine were calculated considering the uncertainties in the values of the energies obtained from the fitting that led to the simulated curve shown in Fig. 6.

3.4. Molecular orbital parameters

Most copper amino acid complexes have the metal ion in elongated octahedral or square planar configurations of negatively charged ligands [24]. The eigenvalues of the $\boldsymbol{g}$ and $\boldsymbol{A}_{Cu}$ tensors given in Table 1 for the case of L-thr:Cu^{2+} indicate an electronic ground orbital state $d_{(x^2-y^2)}$ for the copper ion [25]. Assuming D_{2h} point symmetry of the crystal field, the wave functions of the Cu^{2+} ion can be written as linear combinations of Cu and ligand electronic orbitals [25, 26]:

$$\begin{aligned}
\psi_1(A_g) &= \alpha\left|x^2-y^2\right\rangle - \gamma\Phi_L(A_g),\\
\psi_2(A_g) &= \alpha_1\left|z^2\right\rangle - \gamma_1\Phi_L(A_g),\\
\psi_3(B_{1_g}) &= \beta_1|xy\rangle - \gamma_2\Phi_L(B_{1_g}),\\
\psi_4(B_{2_g}) &= \beta|xz\rangle - \gamma_3\Phi_L(B_{2_g}),\\
\psi_5(B_{3_g}) &= \beta'|yz\rangle - \gamma_4\Phi_L(B_{3_g}),
\end{aligned}\tag{2}$$

where the functions Φ_L represent the ligand group orbitals with the appropriate symmetry. From these wave functions the following spin-Hamiltonian parameters are derived [27]:

$$\begin{aligned}
g_3 &= 2.0023 - 8\alpha^2\beta_1^2\frac{\lambda_0}{E_{xy}},\\
g_2 &= 2.0023 - 2\alpha^2\beta^2\frac{\lambda_0}{E_{xz}},\\
g_1 &= 2.0023 - 2\alpha^2\beta'^2\frac{\lambda_0}{E_{yz}},
\end{aligned}\tag{3}$$

$$\begin{aligned}
\frac{A_{Cu,3}}{P_0} &= \left(-\kappa-\frac{4}{7}\right)\alpha^2+\Delta g_3+\frac{3}{14}(\Delta g_2+\Delta g_1),\\
\frac{A_{Cu,2}}{P_0} &= \left(-\kappa+\frac{2}{7}\right)\alpha^2+\Delta g_2-\frac{3}{14}\Delta g_1,\\
\frac{A_{Cu,1}}{P_0} &= \left(-\kappa+\frac{2}{7}\right)\alpha^2+\Delta g_1-\frac{3}{14}\Delta g_2,
\end{aligned}\tag{4}$$

λ_0 is the Cu^{2+} spin-orbit coupling constant equal to—$829\,cm^{-1}$, κ is the Fermi contact hyperfine constant equal to 0.43 for free Cu(II), $P_0=0.036\,cm^{-1}$ describes the radial extension of the *d*-wave function of the Cu(II) ion, $\Delta g_i=g_i-2.0023$ and E_{ij} are crystal field splittings. The coefficient α^2 and the Fermi constant κ can be evaluated from the hyperfine splitting parameters with Eqs. (3) and (4), using

$$\begin{aligned}
\alpha^2 &= \frac{7}{12}\left[\frac{A_{Cu,1}+A_{Cu,2}-2A_{Cu,3}}{P_0}+2\Delta g_3-\frac{5}{14}(\Delta g_1+\Delta g_2)\right],\\
\kappa &= \frac{1}{\alpha^2}\left[-\frac{A_{Cu,3}}{P_0}-\frac{4}{7}\alpha^2+\Delta g_3+\frac{3}{14}(\Delta g_1+\Delta g_2)\right].
\end{aligned}\tag{5}$$

The coefficients β_i can be evaluated from the *g*-factors and the crystal field energies obtained from the optical absorption spectra. The values obtained are: $\alpha=0.88$, $\beta^2=0.73$, $\beta_1^2=0.62$, $\beta'^2=0.61$ and $\kappa=0.31$, similar to those reported for other copper-doped single crystals [22–24,26]. Combinations with all three $A_{Cu,i}$ having equal

signs, or with $A_{Cu,3}>0$ lead to a large value of the Fermi constant, or to negative parameters, and were not considered. We considered combinations with $A_{Cu,3}<0$, and the parameters listed above are average of these possibilities.

4. Discussion and conclusion

It is well known by crystal growers that the crystal faces with the lowest normal growth rates have the most developed crystal faces and determine the crystal morphology. Thus, the observed change from a habit dominated by {1 1 0} and {1 2 0} faces in pure crystals to one with predominant {2 1 0} faces in the prismatic zone of the doped crystals is a consequence of an inversion in the relative growth velocity of those faces. These results indicate that copper impurities inhibit the normal growth rate of the {2 1 0} faces, making them the most prominent in the doped crystals.

The $3d^9$ electronic configuration of the Cu^{2+} ion can be treated as a $3d^1$ hole configuration with effective electronic spin $S=\frac{1}{2}$, and nuclear spins $I_{Cu}=\frac{3}{2}$ for both natural copper isotopes. The eigenvalues of the $\boldsymbol{g}$ and $\boldsymbol{A}_{Cu}$ tensors obtained from the data given in Table 1 indicate approximate axial symmetry with a distorted square array of ligands. The eigenvectors corresponding to the eigenvalues g_3 and A_3 are similar and define the axial direction. The ground orbital state is predominantly $d_{(x^2-y^2)}$ but should take into account the observed anisotropy of the $\boldsymbol{g}$ and $\boldsymbol{A}_{Cu}$ tensors in the equatorial plane [19]. The principal directions of $\boldsymbol{g}$ and $\boldsymbol{A}_{Cu}$ tensors in the perpendicular plane are different as a consequence of the low symmetry of the copper site. Similar results were obtained by Calvo et al. [17] for Cu^{2+} ions doped L-alanine, whose structure also belongs to the space group $P2_12_12_1$. The analysis of the superhyperfine structure, which is resolved for some orientations of the magnetic field, points to two N ligands in the equatorial plane in *trans* position having hyperfine couplings similar to those measured in other doped Cu-amino acid systems [17, 19, 24, 28].

The site occupied by the Cu^{2+} impurities should have the volume necessary to accommodate the ion and also ligands consistent with the observed EPR spectrum. Inspection of the crystallographic data of Janczak [8] for the undoped crystal allowed us to propose this site as the center of gravity between the atoms N1A, N1D, O2A and O1A, as depicted in Fig. 7, where the Cu^{2+} ion is equatorially bonded to two α amino nitrogens and to two carboxylate oxygens in *trans* coordination, resulting in a distorted square planar arrangement. However, a calculation based in the coordinates of the atoms in the undoped crystal gives distances Cu–N1A = 2.31 Å, Cu–N1D = 2.40 Å, Cu–O1A = 1.61 Å, Cu–O2A = 1.57 Å, with an asymmetry around the Cu^{2+} ion larger than that characteristic for similar copper complexes. It is expected that local distortions occur and generate a new local equilibrium configuration with more standard Cu–N and Cu–O distances, minimizing the elastic energy of the impurity site. The angles N1A–Cu–O1A = 84.2°, N1A–Cu–O2A = 95.1°, N1D–Cu–O1A = 98.7°, N1D–Cu–O2A = 86.9°, calculated from the basic model would also change to approach values closer to 90°. Nevertheless, the values of the crystal field parameters obtained from the optical data indicate that the Cu^{2+} ions are in strongly distorted sites suggesting that the local distortions are not sufficient to produce a more symmetric site. A study of the Cu^{2+} environment using X-ray diffraction is not possible due the high dilution and random distribution of the impurities in the crystal matrix. An accurate analysis of the copper neighborhood could be made only by ENDOR measurements of the nitrogen superhyperfine coupling. The angle between the eigenvector corresponding to g_3 and the normal to the copper equatorial plane defined by the N1A, N1D, O2A and O1A nearest ligands calculated from the structural information [8] is approximately 20° a large value indicating sizeable local distortions at the impurities sites. We emphasize that there are not in the structure of L-threonine other positions which may offer interstitial sites for Cu impurities, having two nitrogen ligands in trans coordination.

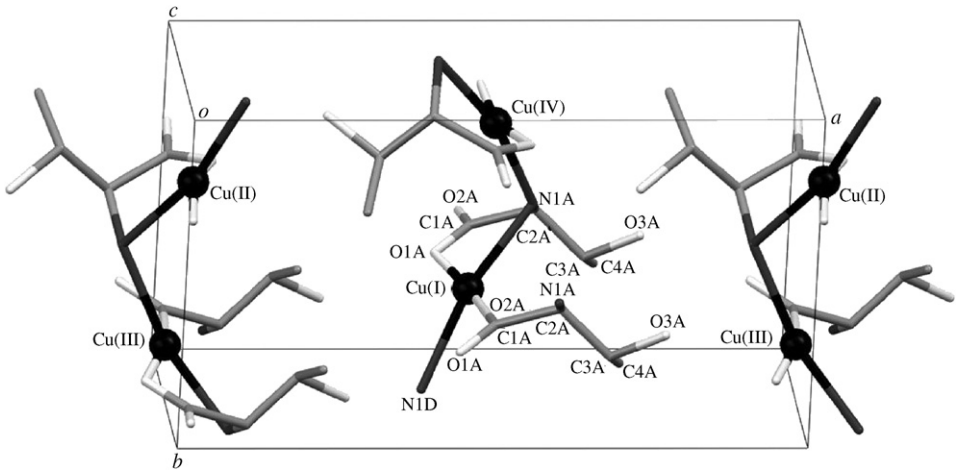

Fig. 7. Site proposed for the Cu^{2+} impurities in the L-threonine structure. The crystallographic data were taken from Janczak et al. [8].

The values of the molecular parameters obtained for copper ions in L-threonine, are similar to those observed for others copper compounds, for example in $CaSIIIiaNO_3$ copper complex [22] and in copper doped cadmium formate dihydrate, $Cd(HCOO)_2\ 2H_2O$ [26], where the copper ions occupy sites having approximate square planar geometry.

Acknowledgments

We thank Dr. O. R. Nascimento (IFSC, USP, Brazil) and Dr. E. M. Lima (UFG, Brazil) for allowing us to use the VARIAN X-band EPR spectrometer and the Cary 50 Spectrophotometer. The work in Brazil was supported by CNPq (472634/2006-2), CAPES, FUNAPE and SECTEC-Go. The work in Argentina was supported by grants CAI+D-UNL, PIP 5274 and ANPCyT PICT 06-13782. RC is a member of CONICET.

References

[1] D. Eimerl, S. Velsko, L. Davis, F. Wang, G. Laiacono, G. Kennedy, IEEE J. Quantum Electron. 25 (1989) 179.
[2] J.J. Rodrigues Jr., L. Misoguti, F.D. Nunes, C.R. Mendonça, S.C. Zilio, Opt. Mater. 22 (2003) 235.
[3] L. Misoguti, A.T. Varela, F.D. Nunes, V.S. Bagnato, F.E.A. Melo, J. Mendes, S.C. Zilio, Opt. Mater. 6 (1996) 147.
[4] S. Dhanuskodi, P.A. Angeli Mary, K. Vasantha, Spectrochim. Acta A 59 (2003) 927.
[5] T. Mallik, T. Kar, J. Cryst. Growth 285 (2005) 178.
[6] M. Ramanadham, S.K. Sikka, R. Chidambaran, Pramana J. Phys. 1 (1973) 247.
[7] D.P. Shoemaker, J. Donohue, V. Schomaker, R.B. Corey, J. Am. Chem. Soc. 72 (1950) 2328.
[8] J. Janczak, D. Zobel, P. Luger, Acta Crystallogr. Sec. C: Cryst. Struct. Commun. 53 (1997) 1901.
[9] G. Ramesh Kumar, S. Gokul Raj, R. Sankar, R. Mohan, S. Pandi, R. Jayavel, J. Cryst. Growth 267 (2004) 213.
[10] A. Pawlukojc, J. Leciejewicz, J. Tomkinson, S.F. Parker, Spectrochim. Acta A 57 (2001) 2513.
[11] B.L. Silva, P.T.C. Freire, F.E.A. Melo, J. Mendes, M.A. Pimenta, M.S.S. Dantas, J. Raman Spectrosc. 31 (2000) 519.
[12] B.L. Silva, P.T.C. Freire, F.E.A. Melo, I. Guedes, M.A.A. Silva, J. Mendes, A.J.D. Moreno, Brazil. J. Phys. 28 (1998) 19.
[13] A.R. Gargaro, L.D. Barron, L. Hecht, J. Raman Spectrosc. 24 (1993) 91.
[14] G. Ramesh Kumar, S. Gokul Raj, R. Mohan, R. Jayavel, Cryst. Growth Des. 6 (2006) 308.
[15] J.R. Pilbrow, Transition ion Electron Paramagnetic Resonance. Clarendon Press, Oxford, 1990.
[16] M. J. Nilges, Thesis, University of Illinois, Urbana, 1979. This program is available for download in 6 〈http://ierc.scs.uiuc.edu/~nilges/software.html〉.
[17] R. Calvo, S.B. Oseroff, H.C. Abache, J. Chem. Phys. 72 (1980) 760.
[18] J.A. Weil, J. Magn. Reson. 18 (1975) 113.
[19] M.B. Massa, S.D. Dalosto, M.G. Ferreyra, G. Labadie, R. Calvo, J. Phys. Chem. A 103 (1999) 2606.
[20] C.J. Ballhausen, Ligand Field Theory, McGraw-Hill, New York, 1962;
C.J. Ballhausen, H.B. Gray, Inorg. Chem. 1 (1962) 111.
[21] M. Salagram, T.S.N. Murthy, K. Hariharan, Cryst. Latt. Def. Amorph. Matter. 17 (1987) 321.
[22] A. Tovar-Tovar, L. Ruiz-Ramírez, A. Campero, A. Romerosa, R. Moreno-Esparza, M.J. Rosales-Hoz, J. Inorg. Biochem. 98 (2004) 1045.
[23] S. Dhanuskodi, P.A. Angeli Mary, P. Sambasiva Rao, Spectrochim. Acta A 61 (2005) 721.
[24] C.A. Steren, R. Calvo, O.E. Piro, B.E. Rivero, Inorg. Chem. 28 (1989) 1933.
[25] B.R. McGarvey, in: R.L. Carlin (Ed.), Transition Metal Chemistry, vol. 3, Dekker, 1966.
[26] S. Kiczka, S.K. Hoffmann, J. Goslar, L. Szczepanska, Phys. Chem. Chem. Phys. 6 (2004) 64.
[27] D. Attanasio, J. Magn. Reson. 26 (1977) 81.
[28] R.C. Santana, J.F. Carvalho, S.R. Amaral, I. Vencato, F. Pelegrini, M.C. Terrile, A.C. Hernandes, R. Calvo, J. Phys. Chem. Sol. 63 (2002) 1857.